ACS OMEGA

http://pubs.acs.org/journal/acsodf

Article

Colorimetric Sensor Based on Ag-Fe NTs for H_2S Sensing

Jiahang Yu, Mingyuan Huang, Huixin Tian, and Xinglian Xu*

Cite This: *ACS Omega* 2022, 7, 44215−44222

Read Online

ACCESS | Metrics & More | Article Recommendations | Supporting Information

ABSTRACT: Meat waste is widely associated with spoilage caused by microbial growth and metabolism. Volatile compounds produced by microbial growth such as volatile sulfides could directly indicate the freshness of meat during distribution and storage. Herein, silver−iron nanotriangles (Ag-Fe NTs) for hydrogen sulfide (H_2S) detection were developed via one-pot facile reflux reactions. The Ag-Fe NTs were integrated into food packaging systems for the rapid, real-time, and nondestructive detection of the freshness of chilled broiler poultry. The principle of color development is that an increase in the volatile sulfide content leads to a change in the absorption wavelength caused by the etching of the Ag-Fe NTs, resulting in a color change (yellow to brown). The minimum H_2S concentrations detected by the naked eye and UV−vis spectrophotometer were 4 and 2 mg/m^3, respectively. This label is economical and practical and can monitor the spoilage of chilled broiler meat products in real-time.

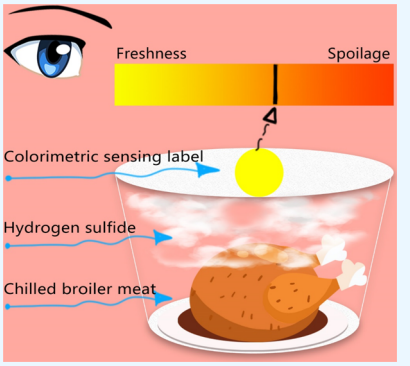

1. INTRODUCTION

Spoilage microorganism is one of the main reasons for food loss and waste, which commonly produce off-odors, off-flavors, discoloration, and slime.[1,2] Therefore, monitoring microbial spoilage during meat storage and transportation has been a worldwide concern. Traditional freshness monitoring mainly relies on end-point inspections, which cannot judge the freshness within the shelf life and cannot meet the demand for circulation and trade. A process for the continuous monitoring of freshness has become imperative for the global meat industry. Intelligent packaging is the best choice to address these challenges. Early research studies have developed specific packaging technologies and techniques including fluorescence spectrometry,[3] Raman spectroscopy,[4] colorimetric,[5] and electrochemistry[6] to monitor the meat storage temperature, pH, and other changes, which can be used to estimate the freshness of meat. However, most methods are not suitable for real-time and on-site analysis, and this strategy of indirect detection suffers from large deviations. Direct monitoring technology reflecting the process and intensity of microbial metabolism can be more accurate in monitoring changes in freshness.[7,8] During meat spoilage, bacterial metabolism produces characteristic spoilage volatile sulfides (H_2S, dimethyl sulfide (DMS, CH_3SCH_3), dimethyl disulfide (DMSS, CH_3SSCH_3), and dimethyl trisulfide (DMSSS, CH_3SSSCH_3)), which has been identified as the main volatiles released during the spoilage of chilled broiler meat.[9,10] Thus, volatile sulfides can directly reflect the freshness of chilled broiler meat. Therefore, real-time monitoring based on characteristic volatile compounds is the main breakthrough in monitoring freshness. The combination of spoilage odor (such as H_2S) and specific materials that present a naked-eye-distinguishable color change would represent a potential breakthrough for monitoring food freshness.

Colorimetric sensors have long been the focus of research studies due to their ability to perform simple, rapid, portable, low-cost, real-time, and nondestructive detection of analytes without complex instrumentation. Thus, colorimetric sensors are becoming widely used for safety and quality monitoring in a variety of industrial processes, such as bioanalytical chemistry, manufacturing, environmental, agriculture, warehousing, food safety, etc.[11−14] Colorimetric sensors aim to detect subtle changes by converting the relevant chemical or physical properties (i.e., temperature, pH value, or molecules) of molecular or ionic species into visible color changes that can be observed by the naked eye. Many efforts have therefore gone into the development of colorimetric sensor systems. Recently, significant progress has been made in nanostructure-based colorimetric sensors using a variety of interesting optical properties of nanostructures.[15] In particular, one of the most striking emerging trends is colorimetric sensing based on the plasmonic coupling (PC)[16] and localized surface plasmon resonance (LSPR)[17] properties of nanoparticles.

It has been widely demonstrated that the intriguing properties of nanoparticles mainly stem from the quantum size effect and surface effect, which can be manipulated in terms of composition, structure, size, shape, and crystal phase.[18,19] Multimetallic nanoparticles composed of different

Received: September 2, 2022
Accepted: November 14, 2022
Published: November 24, 2022

elements demonstrate unique physicochemical properties that are better than those of monometallic nanoparticles in many special applications due to the synergetic effects associated with different metals.[20,21] A promising topic in nanotechnology is the synthesis and stabilization of multimetallic nanoparticles by appropriately combining the different elements of the periodic table. For instance, the coexistence of Ag and Fe in the same nanostructure is interesting for magnetic, optical properties, and catalysis, which opened new opportunities for the design of highly efficient chemical sensor devices. However, due to thermodynamic reasons, the alloying of Ag and Fe is suppressed.[22] Here, we describe the synthesis of Fe-doped Ag NTs via a one-pot approach in a liquid solution, circumventing these thermodynamic limitations. Ag-Fe NTs, also referred to as nanoplates or nanoprisms, are two-dimensional plasmonic nanostructures that have attracted significant attention owing to their strong shape-dependent optical properties.[23] When the lateral dimension of nanotriangles is much larger than the thickness, they possess a high degree of anisotropy, as nanostructures with edges and sharp corners are capable of generating maximum electromagnetic-field enhancement and thus make these nanotriangles appealing as substrates for colorimetric detection, surface-enhanced Raman scattering (SERS) detection, or other spectroscopic techniques.[24] Recent reports have emphasized the unique electronic and optical properties and the multiple applications of multimetallic nanoparticles such as Au-Ag, Au-Ag, and Ag-Fe NPs, were proposed as nanoprobes which are exclusively responsive to sulfide,[25] as plasmonic substrates in surface-enhanced Raman scattering,[26] as well as for use as catalytic materials.[27]

Herein, Ag-Fe NTs were prepared by one-pot facile reflux reactions using silver nitrate ($AgNO_3$) as a silver source, iron(II) D-gluconate dihydrate as an iron source, and carboxymethyl cellulose sodium (CMS) both as a reducing and stabilizing agent. Iron(II) D-gluconate dihydrate and CMS are food additives with excellent safety and biocompatibility.[28] Here, the Ag-Fe NTs are further immobilized in agar powder gels to produce a colorimetric sensor, which can detect a wide range of volatile sulfides. This can then be applied to the detection of toxic gases to produce a significant color change. Its color changes due to various chemical interactions with the analyte.

This study developed an Ag-Fe NT-based colorimetric sensor to monitor the freshness of meat at different temperatures through chemical interactions with volatile sulfides. The resulting color changes are easily distinguished by the human eye. The method would represent a significant advancement in monitoring meat freshness. The system is cost-effective, nondestructive, selective, sensitive, and accurate.

2. MATERIALS AND METHODS

2.1. Materials and Reagents. Carboxymethyl cellulose sodium (CMS), iron(II) D-gluconate dihydrate, silver nitrate ($AgNO_3$), agar powder, hydrochloric acid (HCl), sodium sulfide nonahydrate ($Na_2S{\cdot}9H_2O$), and all of the other flavor substances were purchased from Shanghai Yuanye Bio-Technology Co., Ltd. Tyvek paper and foam tape (1600T) were purchased from Beijing 3M Co., Ltd. Chilled broiler meat was purchased from Jiangsu Lihua Animal Husbandry Co., Ltd.

2.2. Synthesis of Ag_x-Fe_{2-x} NTS. CMS (0.1 g) was added to ultrapure water (98 mL) and stirred for 10 min. This was followed by the addition of the $AgNO_3$ solution (6×10^{-2} M, 1 mL) and iron(II) D-gluconate dihydrate solution (14×10^{-2} M, 1 mL). The mixture was then incubated in a water bath at 80 °C for 8 h until a yellow $Ag_{0.6}$-$Fe_{1.4}$ NT solution was generated. By altering the amount of $AgNO_3$ and the amount of the iron(II) D-gluconate dihydrate, Ag_x-Fe_{2-x} NTs with different particle sizes were synthesized. The Ag_x-Fe_{2-x} NT solutions were stored in the refrigerator at 4 °C until use.

2.3. Preparation of Colorimetric Sensing Label. Preparation of colorimetric gel: agar powder (1 g) was added to ultrapure water (50 mL) and stirred at 100 °C for 1 h until complete dissolution. This was followed by the addition of $Ag_{0.6}$-$Fe_{1.4}$ NT solution (50 mL) and stirred at 100 °C for 2 min. Following solidification at room temperature, which was cut into 2 mm high cylinders (diameter = 15 mm).

Typical preparation of colorimetric gel tank was prepared by consulting our previously published papers with some modifications.[29] The colorimetric gel tank is made of ring-shaped foam tape with a 25 mm outer ring radius and a 15 mm inner ring radius. The bottom was sealed with Tyvek paper, which has excellent breathability and safety. The colorimetric gel is put in the colorimetric gel tank to obtain a colorimetric sensing label.

2.4. Detection of Gaseous Hydrogen Sulfide. A simple laboratory-made device for the production of gaseous H_2S was assembled. The Ag_x-Fe_{2-x} NT liquid was added to a 2 mL centrifuge tube (without capping), following which the centrifuge tube was fixed inside a 1 L container with double-sided tape. The container was then sealed after filling with 20% CO_2 and 80% N_2. The Na_2S and HCl solutions were subsequently injected into the container separately using a syringe, and the pinhole was sealed. H_2S gas was generated at room temperature by mixing solutions of Na_2S with HCl, in which the molar concentration of HCl was thrice that of Na_2S. Excess HCl in the solution helps prevent the diffusion of the formed H_2S back into the solution, ensuring a presumably quantitative formation of H_2S gas. Although the exact concentration of the generated H_2S gas is unknown, the concentration provided below is the highest, depending on the amount of sodium sulfide used.

2.5. Detection of TVCs. Total viable counts (TVCs) were determined according to the China National Food Safety Standard methods Food microbiological examination (GB 4789.2-2016). The TVCs were determined using Plate Count Agar (PCA, Land Bridge, Beijing, China) after incubation for 10 days at 4 °C.

2.6. Structural Characterization of $Ag_{0.6}$-$Fe_{1.4}$ NTs. Dynamic light scattering (DLS) and ζ-potential measurements were recorded on Zetasizer Nano ZS90 (Zeta sizer Nano, Malvern, U.K.). UV−vis absorption spectra were measured on a SpectraMax M2 microplate reader (Molecular Devices, Sunnyvale, CA). Transmission electron microscopy (TEM) images were acquired using a JEM-2100F microscope (TEM, JEM-2100F, JEOL, Tokyo, Japan).

2.7. Headspace and Gas Chromatography−Mass Spectrometry (GC/MS) Analysis. Volatile compound analysis was performed on a TRACE GC Ultra gas chromatography coupled with a TriPlus autosampler and a DSQ II mass selective detector (Thermo Scientific, Massachusetts). Five grams of chilled broiler meat and 5 μL of internal standard (2-cyclohexanone dissolved in absolute ethanol, final concentration 5 mg/m^3) were loaded into a 20 mL headspace bottle (ANPEL Laboratory, Shanghai, China), and the headspace bottle was sealed with a Teflon septum and an

https://doi.org/10.1021/acsomega.2c05682
ACS Omega 2022, 7, 44215−44222

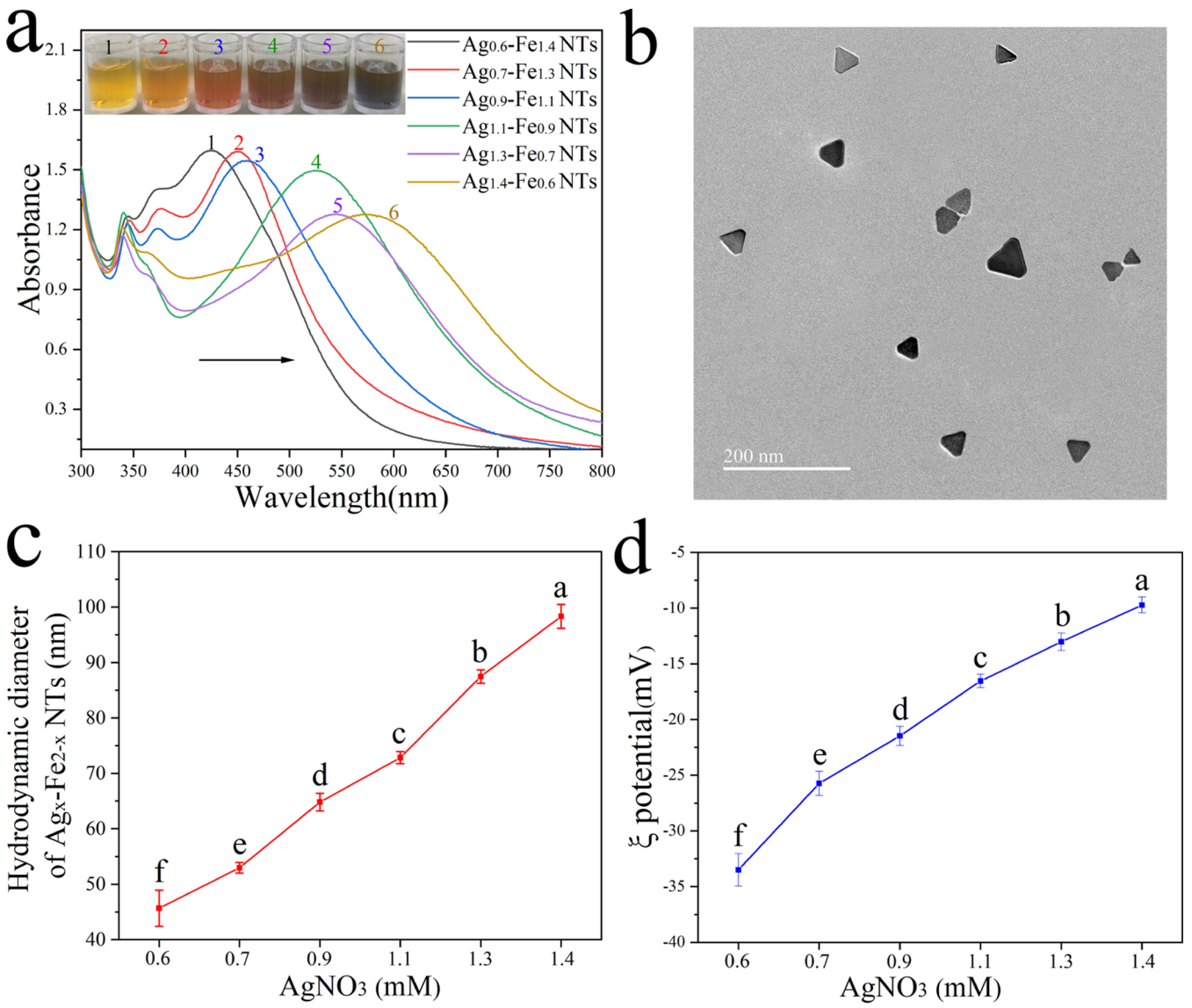

Figure 1. (a) Digital photographs and UV−vis spectra. (b) TEM image of $Ag_{0.6}$-$Fe_{1.4}$ NTs. Hydrodynamic diameter (c) and ζ-potential (d) of different Ag_x-Fe_{2-x} NTs. Vertical bars represent the standard deviation of mean (n = 6). Significance was considered at $P < 0.05$.

aluminum cap (Hua Guan, Shanghai, China). Then, the headspace bottle was incubated at 40 °C for 30 min in an orbital shaker with a shaking speed of 150 rpm. Then, the solid-phase microextraction (SPME) fiber was exposed to the headspace for another 30 min under the same conditions. The length of the SPME fiber in the headspace was kept constant. After extraction, the SPME fiber was desorbed into the GC injector at 250 °C for 3 min in splitless mode. The headspace volatiles were separated on a TR-5 MS capillary column (30 m length × 0.25 mm i.d. × 025 μm film thickness; Thermo Scientific, Massachusetts) with 1 mL/min constant helium flow in splitless mode. The temperature program was 40 °C for 3 min, then a ramp of 10 °C/min until 95 °C, followed by a ramp of 30 °C/min to 220 °C, and maintained for 3 min. The mass spectrometer was operated in electron impact (EI) mode (70 eV), and the mass scan range of m/z 29−450. Identification of the volatile components was performed by comparing the mass spectra with the data system library (NIST/EPA/NIH). The contents of volatiles were quantified by peak areas in the total ion chromatogram.

3. RESULTS AND DISCUSSION

3.1. Synthesis and Characterization of Ag_x-Fe_{2-x} NTs.

The LSPR of size-selected Ag_x-Fe_{2-x} (x = 0.6, 0.7, 0.9, 1.1, 1.3, 1.4) NTs, prepared by one-pot facile reflux reactions, were investigated experimentally and theoretically. As shown in Figure 1a, $Ag_{0.6}$-$Fe_{1.4}$ NTs were produced with a sharp plasmonic peak at around 424 nm. Increasing the $AgNO_3$ concentration from 0.6 mM to 1.4 mM gradually red-shifted the absorption peak of the products from ∼424 to 574 nm. Figure 1a shows the corresponding digital photographs of the Ag_x-Fe_{2-x} NTs exhibiting bright colors of yellow, bright yellow, brown, dark brown, purple, and blue. TEM measures the diameter of the metallic core and DLS measures the hydrodynamic diameter, which is influenced by surface ligands and stabilizing agents. Thus, the hydrodynamic diameter was slightly larger than the diameter measured from TEM images but follow similar trends. TEM images of $Ag_{0.6}$-$Fe_{1.4}$ NTs reveal that nanotriangle structures have been formed (Figure 1b). The physicochemical properties of NTs are mainly accounted for in their hydrodynamic diameter and ζ-

https://doi.org/10.1021/acsomega.2c05682
ACS Omega 2022, 7, 44215−44222

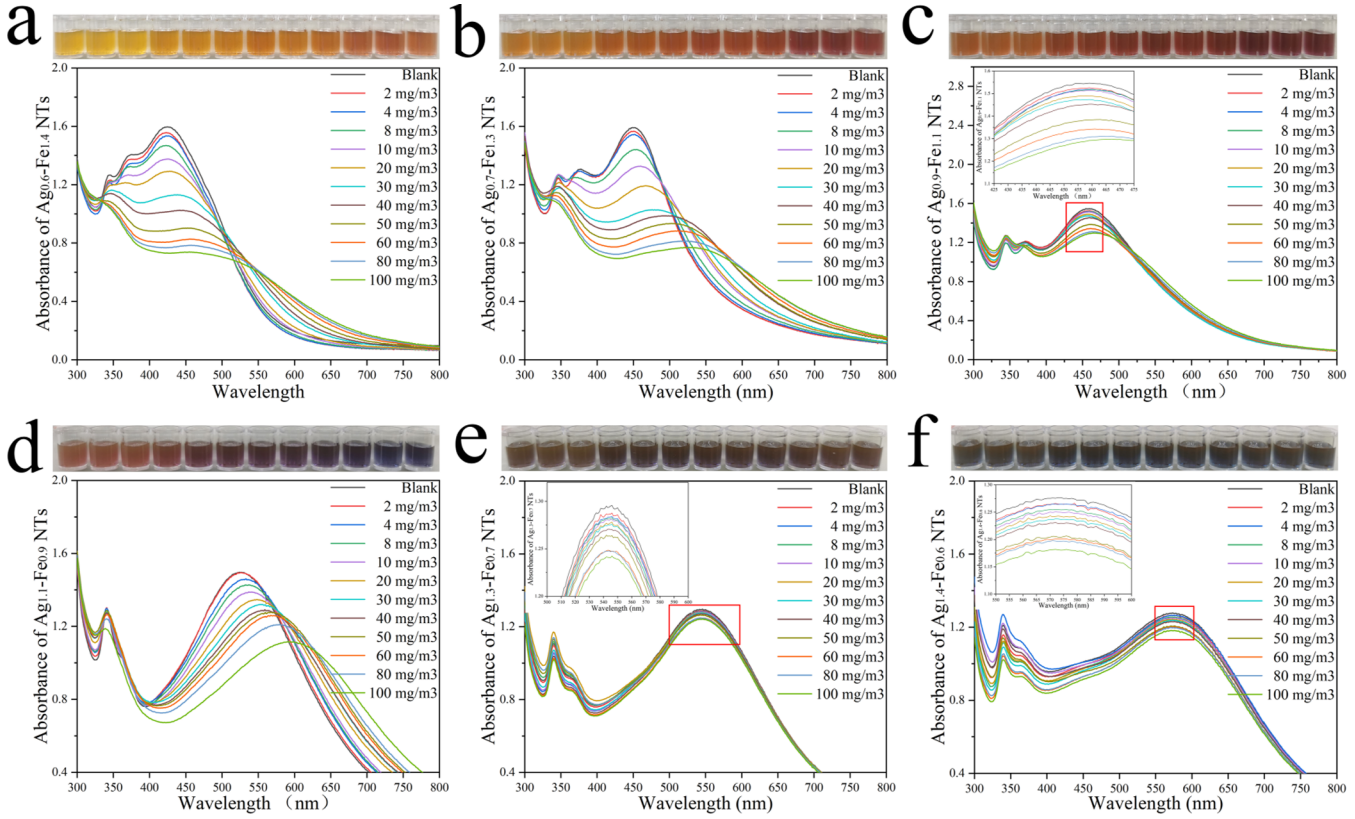

Figure 2. Digital photographs and UV−vis spectra of different Ag_x-Fe_{2-x} NTs exposed to H_2S at different concentrations: (a) $Ag_{0.6}$-$Fe_{1.4}$ NTs, (b) $Ag_{0.7}$-$Fe_{1.3}$ NTs, (c) $Ag_{0.9}$-$Fe_{1.1}$ NTs, (d) $Ag_{1.1}$-$Fe_{0.9}$ NTs, (e) $Ag_{1.3}$-$Fe_{0.7}$ NTs, and (f) $Ag_{1.4}$-$Fe_{0.6}$ NTs.

potential.[30] DLS was used to measure the hydrodynamic diameter of Ag_x-Fe_{2-x} NTs (Figure 1c); the results suggested a drastic increase in the Ag_x-Fe_{2-x} NT size from the initial value of 45.657 nm (0.6 mM) to 98.325 nm (1.4 mM) and simultaneously assembled into aggregates with the increasing $AgNO_3$ concentration (Figure 1c). The red-shift of the spectra can, therefore, be attributed to the SPR coupling[31,32] among neighboring Ag_x-Fe_{2-x} NTs. Increasing the $AgNO_3$ concentration significantly promoted the growth and assembly of Ag_x-Fe_{2-x} NTs. As shown in Figure 1d, the ζ-potential of Ag_x-Fe_{2-x} NTs changes from −33.494 to −9.72 mV with the increasing $AgNO_3$ concentration, indicating a decrease in surface charge and hence a decrease in the ligand coverage density on the Ag_x-Fe_{2-x} NT surface. This confirmed that when the $AgNO_3$ concentration was increased, the Ag_x-Fe_{2-x} NTs can progressively increase in size and simultaneously decrease the ligand density on their surfaces.

3.2. Optimization of the Assay. Different ratios of ligands on the surface of NTs also determine the distance between particles, which, in turn, controls the plasmonic coupling of the Ag_x-Fe_{2-x} NTs and the color of the solution.[33−35] Without using any instrument, it is easy for the naked eye to distinguish the color change. As shown in Figure 2a, $Ag_{0.6}$-$Fe_{1.4}$ NTs react with the increasing concentrations of H_2S, changing the color of the solution to yellow and finally brown; further, the plasmonic peak originally at ∼346 and ∼376 nm gradually decreases in intensity and eventually disappears, indicating that Ag_x-Fe_{2-x} NTs are gradually etched by H_2S and eventually no longer have a triangular structure (Supporting Information Figure S1). All these results suggest that the sensing relies on the fact that H_2S reacts with Ag-Fe NTs to form Ag_2S-Fe NTs, thus inducing apparent color and spectral changes (Scheme 1). The reaction occurs as follows

$$2Ag^+ + S^{2-} = Ag_2S \quad (1)$$

Scheme 1. Sensing Mechanism of the Proposed Assay

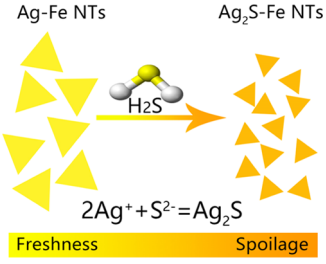

To obtain the best sensing performance of Ag_x-Fe_{2-x} NTs for H_2S detection based on the gradient of color change and sensitivity, Ag_x-Fe_{2-x} NTs with different hydrodynamic diameters and surface charges were evaluated for H_2S sensing. The color sensitivity of Ag_x-Fe_{2-x} NTs is directly related to their surface charge. A relatively low ζ-potential reduces the stability of Ag_x-Fe_{2-x} NTs, resulting in a higher H_2S reaction sensitivity. A higher surface charge implies a smaller hydrodynamic diameter. If the size of Ag_x-Fe_{2-x} NTs is too large, the detection range will be widened and the sensitivity will be lowered.[36] As shown in Figure 2, as the particle size of the Ag_x-Fe_{2-x} NTs increases, the sensitivity of the reaction increases and the color change becomes more pronounced. However,

https://doi.org/10.1021/acsomega.2c05682
ACS Omega 2022, 7, 44215−44222

excessive oversizing might lead to negative results as well. The sensitivity of $Ag_{1.3}$-$Fe_{0.7}$ NTs and $Ag_{1.4}$-$Fe_{0.6}$ NTs severely decreased, and the color change cannot be observed visually by the naked eye. The minimum H_2S concentrations detected by the naked eye and UV−vis spectrophotometer were 4 and 2 mg/m^3, respectively, which were the lowest or equivalent of those reported by other colorimetric methods.[37−40] The size of the Ag_x-Fe_{2-x} NTs was fixed at 8.04 nm for further testing ($Ag_{0.6}$-$Fe_{1.4}$ NTs). The reproducibility of the method was evaluated by analyzing six replicates of H_2S at 50 ppm, and the relative standard deviation was 3.2%.

3.3. Selectivity Test. HS/SPME-GC/MS analysis revealed 45 volatile compounds (VOCs) that were present during the storage of chilled broiler meat under 4 °C and modified atmosphere packaging conditions (Table S1). Including sulfurous compounds, hydrocarbons, alcohols, phenols, aldehydes, ketones, acids, esters, and nitrogenous compounds. To evaluate the feasibility of this as-proposed sensing method-based $Ag_{0.6}$-$Fe_{1.4}$ NTs for accurate reporting of sulfurous compound levels in actual samples, several representative compounds were evaluated under the same reaction conditions as described above. As shown in Figure 3, verification of the

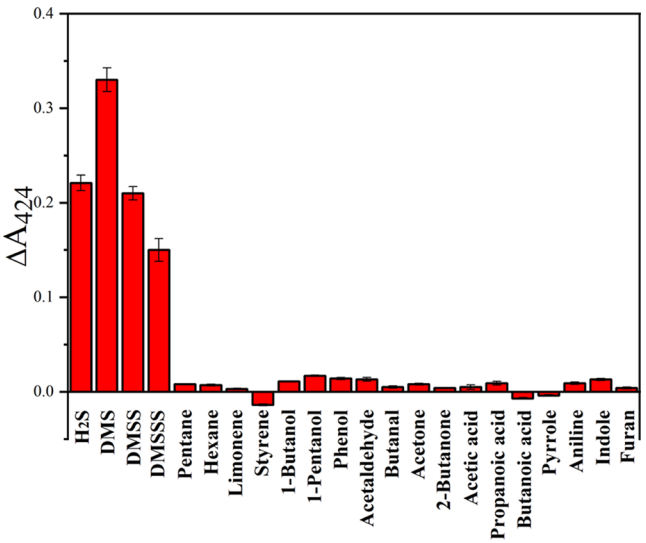

Figure 3. Decreased absorbance of $Ag_{0.6}$-$Fe_{1.4}$ NTs at 424 nm upon reaction with sulfurous compounds or interfering compounds (H_2S, DMS, DMSS, DMSSS: 10 mg/m^3; pentane, hexane, limonene, styrene, 1-butanol, 1-pentanol, phenol, acetaldehyde, butanal, acetone, 2-butanone, acetic acid, propanoic acid, butanoic acid, pyrrole, aniline, indole, furan: 50 mg/m^3). Each data point is the mean of six replicate samples (mean ± standard deviation). Vertical bars represent the standard deviation of the mean. Significance was considered at $P < 0.05$.

reaction using sulfurous compounds and other VOCs confirmed that sulfurous compounds could produce a visible color change and the absorbance decreases at 424 nm. In contrast, after the introduction of other VOCs, no color change was observed, and all compounds occurred at a higher concentration than sulfurous compounds. Of particular mention was the $Ag_{0.6}$-$Fe_{1.4}$ NTs exhibit less response to butanal, 2-butanone, acetic acid, pyrrole, and aniline. These compounds have a strong complexing ability, such that when a probe with $Ag_{0.6}$-$Fe_{1.4}$ NTs is used, the $Ag_{0.6}$-$Fe_{1.4}$ NTs can be etched to interfere with the detection of sulfurous compounds. All these results demonstrate that the compounds tested have negligible effects on sulfurous compound sensing and that the proposed method has high selectivity for sulfurous compounds. Based on such acceptable sensing performances, $Ag_{0.6}$-$Fe_{1.4}$ NTs exhibited a great potential to be directly employed as a sensor for the accurate detection of sulfurous compounds in actual food media.

3.4. Immobilization of $Ag_{0.6}$-$Fe_{1.4}$ NTs in Agar as a Colorimetric Sensing Label. To facilitate the broader application of the proposed method, $Ag_{0.6}$-$Fe_{1.4}$ NTs were fixed into agar powder gels to produce a solid form of the colorimetric gel. Agar powder is somewhat chemically inert and does not react with $Ag_{0.6}$-$Fe_{1.4}$ NTs. As shown in Figure 4a, the colorimetric gel exhibited color changes from yellow to dark brown with increasing concentrations of H_2S similar to those observed in the solution, suggesting their applicability for H_2S detection. It is worth noting that these colorimetric gels can detect H_2S at lower concentrations than that in solution. This can be explained by the fact that agar powder is composed of organic polysaccharides with abundant water and is able to adsorb and preconcentrate sulfides in samples. The UV−vis spectra of agar powder gels incubated with different concentrations of H_2S are shown in Figure 4b. Under the optimal conditions, A_{475} of the colorimetric gel decreased gradually with the increasing H_2S concentration. There is a linear relationship between ΔA_{475} and H_2S concentration (Figure 4c). The linear regression equations are $\Delta A_{475} = 0.03823 + 0.00638C$ ($n = 5$, $R^2 = 0.98716$). The colorimetric sensing label was made of colorimetric gel and a colorimetric gel tank. The colorimetric gel tank can protect the colorimetric gel from leaking or contacting the meats while still in contact with the sulfurous compound produced in the chilled broiler meat in the modified atmosphere packaging. During the experiment on chilled broiler meat spoilage, the colorimetric sensing label was attached to packaging film inside the modified atmosphere packaging box and showed a clear color change that was suitable for monitoring the freshness of chilled broiler meat with the naked eye (Supporting Information Figure S2). However, to achieve a quantitative evaluation of the freshness of chilled broiler meat using the colorimetric sensing label, we explored methods to convert colors to numerical values.

The RGB (red, green, and blue) model, which uses transmitted light to represent colors, is the most commonly used color model in the color measurement of digital images. Digital color images of the freshness indicators of the colorimetric sensing labels were regularly recorded with a Canon EOS 700D digital camera. The images were imported into Adobe Photoshop 2020 software, and the average RGB pixel intensities were collected. All RGB images of the colorimetric sensing labels were captured three times, and the final RGB values were determined by averaging the individual RGB values. As shown in Supporting Information Figure S2, the colorimetric sensing label in chilled broiler meat wrapped in modified atmosphere packaging (packaging machine SMART500, 20% CO_2, 80% N_2) at 4 °C exhibited color changes from yellow to brown and dark brown, similar to those observed in solution. The R and G values of the colorimetric sensing label showed a significant decrease when the colorimetric sensing label was used to monitor chilled broiler meat spoilage (the weight of each sample is 500 ± 5 g), while the B values did not present regular changes (Figure 4g−i). The experiment also verified the color change of the

https://doi.org/10.1021/acsomega.2c05682
ACS Omega 2022, 7, 44215−44222

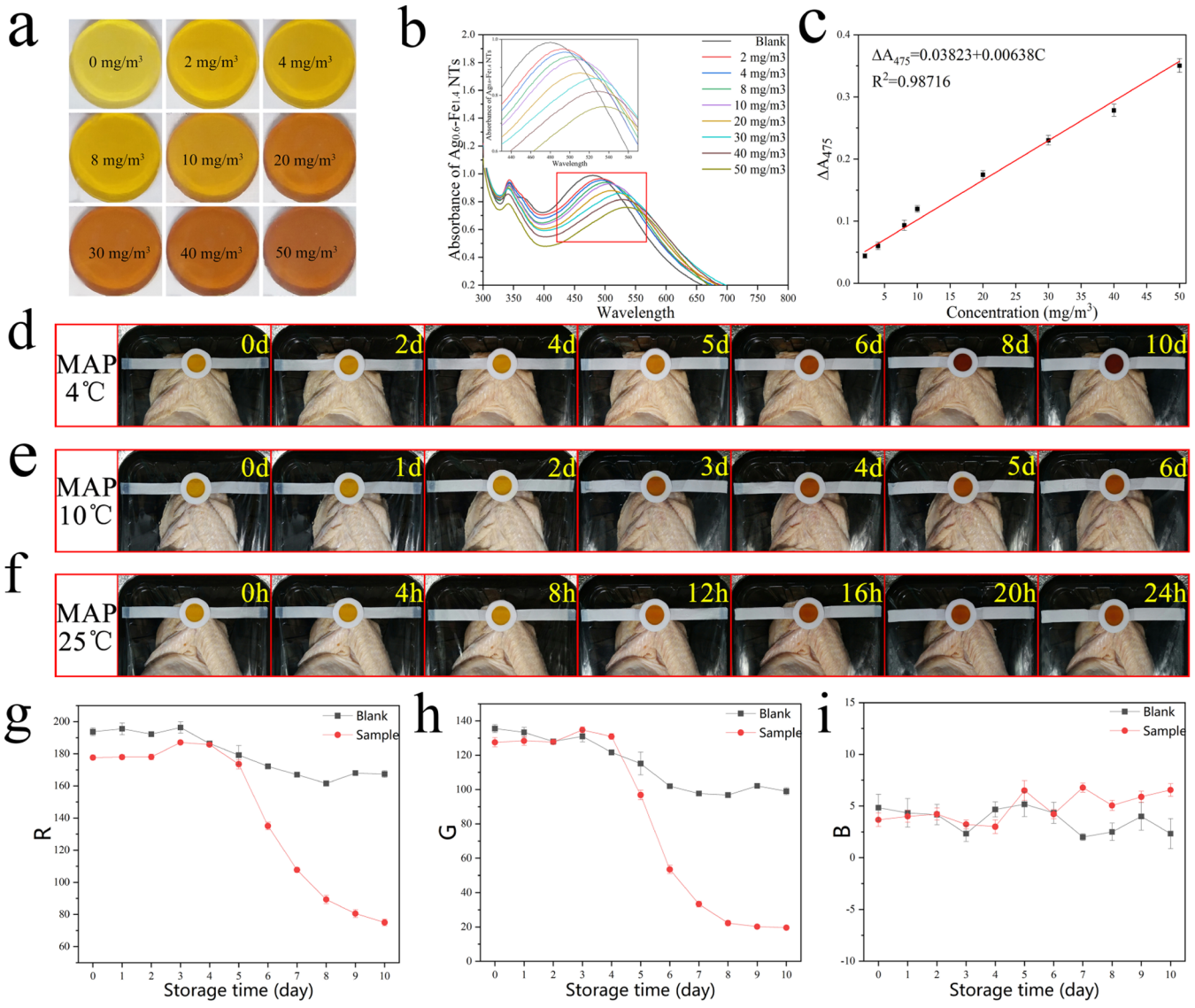

Figure 4. (a) Photographs of agar powder gels incubated with different concentrations of H_2S. (b) UV−vis spectra of agar powder gels incubated with different concentrations of H_2S. (c) Relationship between the concentrations of H_2S and ΔA_{475}. The error bars show the standard deviation of quintuplicate tests ($N = 5$). (d−f) Color change in colorimetric sensing labels in chilled broiler meat wrapped in modified atmosphere packaging at different temperatures of (d) 4 °C, (e) 10 °C, (f) 25 °C and R (g), G (h), and B (i) values for color change in the colorimetric sensing label. Each data point is the mean of six replicate samples (mean ± standard error). Vertical bars represent the standard error of mean.

colorimetric sensing label in chilled broiler meat modified atmosphere packaging (MAP: 20% CO_2, 80% N_2) under different storage temperatures (10 and 25 °C). The results show that the color change time is advanced when the temperature rises (Figure 4d−f).

Over time, the microbiological parameters of packaged chilled broiler meat related to their quality, such as TVCs, undergo changes. The chemical spoilage index values derived from the minimum spoilage levels of specific spoilage microorganisms showed that the acceptable limit for human consumption is under 7.0 log CFU g^{-1} of microorganisms in chilled broiler meat.[41] As shown in Figure 5, the TVC levels were 3.45 log CFU g^{-1} and increased with an increase in the storage time. Furthermore, the TVC levels exceeded the threshold value of 7.0 log CFU g^{-1} in approximately six days at 4 °C. As shown in Supporting Information Figure S2, when the chilled broiler meat was very fresh at storage temperatures at 4 °C, the color of the colorimetric sensing label was bright yellow, which indicated that the meat in the package would have its best flavor. The color change from bright yellow to light brown occurred at 6 days, which is consistent with the minimum spoilage-level data at 4 °C. As expected, the as-prepared colorimetric sensing label showed a good response to microbiological parameter changes in chilled broiler meat during storage. Furthermore, the visual inspection did not indicate any differences in the colors of the blank sample stored at 4 °C (the blank sample was prepared by adding pure water).

Based on the above results, it can be concluded that the colorimetric sensing label designed in this study is highly promising as a freshness monitor. Therefore, consumers or retailers can not only judge the freshness of chilled broiler meat with the naked eye but also assess its freshness level based on RGB values extracted from colorimetric sensing label images.

https://doi.org/10.1021/acsomega.2c05682
ACS Omega 2022, 7, 44215−44222

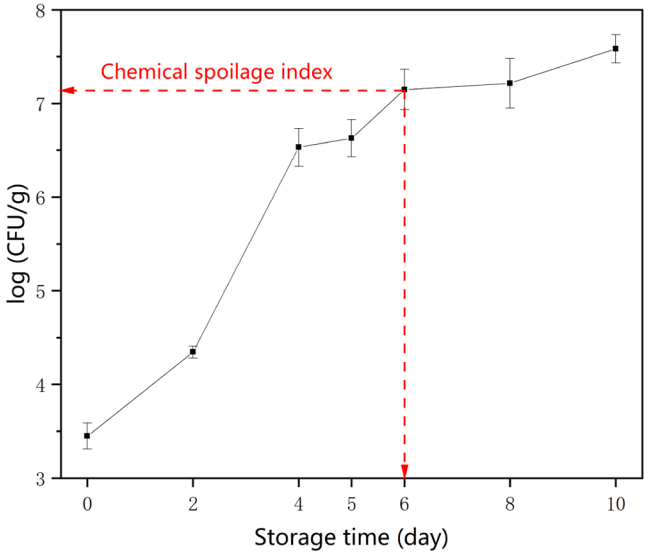

Figure 5. Changes in TVC in packaged chilled broiler meat stored at 4 °C.

4. CONCLUSIONS

In summary, a nondestructive, easy-to-implement colorimetric sensing label for volatile sulfides detection based on Ag-Fe NTs was developed for a rapid, real-time, and low-cost detection of chilled broiler meat spoilage, which gives a sharp-contrast bright yellow-to-brown color change. The developed colorimetric sensing label responded to the freshness of packaged chilled broiler meat changes and perform reliably as freshness-history recorders through irreversible color changes, which was found to operate on a similar timescale to chilled broiler meat-spoilage processes at 4 °C. Because the surface ligands are food additives with excellent biocompatibility and safety, the colorimetric sensing label is nontoxic and eco-friendly. Furthermore, this colorimetric sensing label has wider applicability in many other food packaging systems such as eggs, dairy products, meat, and vegetables as they may also emit volatile sulfides and may have great potential to revolutionize the current food packages.

■ ASSOCIATED CONTENT

Supporting Information

The Supporting Information is available free of charge at https://pubs.acs.org/doi/10.1021/acsomega.2c05682.

TEM image, color change of colorimetric sensing label, and volatile organic compounds (VOCs) (PDF)

■ AUTHOR INFORMATION

Corresponding Author

Xinglian Xu − *Key Laboratory of Meat Processing, Ministry of Agriculture, Key Lab of Meat Processing and Quality Control, Ministry of Education, Jiangsu Collaborative Innovation Center of Meat Production and Processing, College of Food Science and Technology, Nanjing Agricultural University, Nanjing 210095, China*; Phone: +86 025 84395939; Email: xlxus@njau.edu.cn; Fax: +86 025 84395730

Authors

Jiahang Yu − *Key Laboratory of Meat Processing, Ministry of Agriculture, Key Lab of Meat Processing and Quality Control, Ministry of Education, Jiangsu Collaborative Innovation Center of Meat Production and Processing, College of Food Science and Technology, Nanjing Agricultural University, Nanjing 210095, China*; orcid.org/0000-0003-4352-8991

Mingyuan Huang − *Key Laboratory of Meat Processing, Ministry of Agriculture, Key Lab of Meat Processing and Quality Control, Ministry of Education, Jiangsu Collaborative Innovation Center of Meat Production and Processing, College of Food Science and Technology, Nanjing Agricultural University, Nanjing 210095, China*

Huixin Tian − *Key Laboratory of Meat Processing, Ministry of Agriculture, Key Lab of Meat Processing and Quality Control, Ministry of Education, Jiangsu Collaborative Innovation Center of Meat Production and Processing, College of Food Science and Technology, Nanjing Agricultural University, Nanjing 210095, China*

Complete contact information is available at: https://pubs.acs.org/10.1021/acsomega.2c05682

Author Contributions

J.Y. was responsible for the methodology, data curation, investigation, conceptualization, and writing the original draft. M.H. managed the provision of study materials and writing of the review and editing. H.T. was responsible for the provision of study materials. X.X. handled the methodology, writing of the review and editing, and funding acquisition.

Notes

The authors declare no competing financial interest.

■ ACKNOWLEDGMENTS

The study was supported by the China Agriculture Research System of MOF and MARA (CARS-41). A Project Funded by the Priority Academic Program Development of Jiangsu Higher Education Institutions (PAPD).

■ REFERENCES

(1) Hayat, M. N.; Kaka, U.; Sazili, A. Q. Assessment of Physicochemical Characteristics and Microbiological Quality in Broiler Chicken Breast Muscle (Pectoralis major) Subjected to Different Temperatures and Lengths of Cold Transportation. *Foods* **2021**, *10*, 874.

(2) Echegaray, N.; Pateiro, M.; Munekata, P. E. S.; Lorenzo, J. M.; Chabani, Z.; Farag, M. A.; Domínguez, R. Measurement of Antioxidant Capacity of Meat and Meat Products: Methods and Applications. *Molecules* **2021**, *26*, 3880.

(3) Zhao, Y.; Shi, C.; Yang, X.; Shen, B.; Sun, Y.; Chen, Y.; Xu, X.; Sun, H.; Yu, K.; Yang, B.; Lin, Q. pH- and Temperature-Sensitive Hydrogel Nanoparticles with Dual Photoluminescence for Bioprobes. *ACS Nano* **2016**, *10*, 5856−5863.

(4) Katemala, S.; Molee, A.; Thumanu, K.; Yongsawatdigul, J. A comparative study of meat quality and vibrational spectroscopic properties of different chicken breeds. *Poult. Sci.* **2022**, *101*, No. 101829.

(5) He, Y.; Lu, L.; Lin, Y.; Li, R.; Yuan, Y.; Lu, X.; Zou, Y.; Zhou, W.; Wang, Z.; Li, J. Intelligent pH-sensing film based on polyvinyl alcohol/cellulose nanocrystal with purple cabbage anthocyanins for visually monitoring shrimp freshness. *Int. J. Biol. Macromol.* **2022**, *218*, 900−908.

(6) Li, Z.; Wang, Z.; Li, J.; Zhu, Q.; Wang, Z.; Dai, Z. Enhancing Photoelectric Response of an Au@Ag/AgI Schottky Contact through Regulation of Localized Surface Plasmon Resonance. *J. Am. Chem. Soc.* **2021**, *143*, 13478−13482.

(7) Guo, Z.; Ge, X.; Li, W.; Yang, L.; Han, L.; Yu, Q.-l. Active-intelligent film based on pectin from watermelon peel containing

beetroot extract to monitor the freshness of packaged chilled beef. *Food Hydrocolloids* **2021**, *119*, No. 106751.
(8) Kim, D.; Cao, Y.; Mariappan, D.; Bono, M. S., Jr; Hart, A. J.; Marelli, B. A Microneedle Technology for Sampling and Sensing Bacteria in the Food Supply Chain. *Adv. Funct. Mater.* **2021**, *31*, No. 2005370.
(9) Lovestead, T. M.; Bruno, T. J. Detection of poultry spoilage markers from headspace analysis with cryoadsorption on a short alumina PLOT column. *Food Chem.* **2010**, *121*, 1274−1282.
(10) Yuan, Z.; Bariya, M.; Fahad, H. M.; Wu, J.; Han, R.; Gupta, N.; Javey, A. Trace-Level, Multi-Gas Detection for Food Quality Assessment Based on Decorated Silicon Transistor Arrays. *Adv. Mater.* **2020**, *32*, No. 1908385.
(11) Srivastava, M.; Srivastava, S. K.; Prakash Ojha, R.; Prakash, R. Smartphone-assisted Colorimetric Sensor based on Nanozyme for On-Site Glucose Monitoring. *Microchem. J.* **2022**, *182*, No. 107850.
(12) Han, D.; Yang, H.; Zhou, Z.; Wu, K.; Ma, J.; Fang, Y.; Hong, Q.; Xi, G.; Liu, S.; Shen, Y.; Zhang, Y. Photoelectron Storages in Functionalized Carbon Nitrides for Colorimetric Sensing of Oxygen. *ACS Sens.* **2022**, *7*, 2328.
(13) Lee, J.; Noh, H.; Lee, C.-J.; Bae, J.-H.; Baek, M.-C.; Choi, M.; Nam, S.-W.; Cha, H.-H.; Chong, G. O.; Han, H. S.; Park, H. Diagnosis of pathogen infection via a multiple-wavelength colorimetric sensor platform with loop-mediated isothermal amplification. *Sens. Actuators, B* **2022**, *370*, No. 132449.
(14) Jung, D. H.; Kim, Y.; Cho, H. H.; Lee, B.; Suh, S.-J.; Heo, J. H.; Lee, J. H. Automatic quantification of living cells via a non-invasive achromatic colorimetric sensor through machine learning-assisted image analysis using a smartphone. *Biochem. Eng. J.* **2022**, *450*, No. 138281.
(15) Heuer-Jungemann, A.; Feliu Torres, N.; Bakaimi, I.; Hamaly, M.; Alkilany, A.; Chakraborty, I.; Masood, A.; Casula, M.; Kostopoulou, A.; Oh, E.; Susumu, K.; Stewart, M.; Medintz, I.; Stratakis, E.; Parak, W.; Kanaras, A. The Role of Ligands in the Chemical Synthesis and Applications of Inorganic Nanoparticles. *Chem. Rev.* **2019**, *119*, 4819.
(16) Wang, Q.; Domen, K. Particulate Photocatalysts for Light-Driven Water Splitting: Mechanisms, Challenges, and Design Strategies. *Chem. Rev.* **2019**, *120*, 919.
(17) Ratchford, D. C. Plasmon-Induced Charge Transfer: Challenges and Outlook. *ACS Nano* **2019**, *13*, 13610−13614.
(18) Chung, D. Y.; Yoo, J. M.; Sung, Y.-E. Highly Durable and Active Pt-Based Nanoscale Design for Fuel-Cell Oxygen-Reduction Electrocatalysts. *Adv. Mater.* **2018**, *30*, No. 1704123.
(19) Gamler, J. T. L.; Ashberry, H. M.; Skrabalak, S. E.; Koczkur, K. M. Random Alloyed versus Intermetallic Nanoparticles: A Comparison of Electrocatalytic Performance. *Adv. Mater.* **2018**, *30*, No. 1801563.
(20) Wang, L.; Holewinski, A.; Wang, C. Prospects of Platinum-Based Nanostructures for the Electrocatalytic Reduction of Oxygen. *ACS Catal.* **2018**, *8*, 9388−9398.
(21) Bu, L.; Shao, Q.; Pi, Y.; Yao, J.; Luo, M.; Lang, J.; Hwang, S.; Xin, H.; Huang, B.; Guo, J.; Su, D.; Guo, S.; Huang, X. Coupled s-p-d Exchange in Facet-Controlled Pd3Pb Tripods Enhances Oxygen Reduction Catalysis. *Chem* **2018**, *4*, 359−371.
(22) Srivastava, C.; Sushma, K. V. L. Compositionally Graded Microstructure for Ag-Fe Nanoparticles. *Nano-Micro Lett.* **2012**, *4*, 172−175.
(23) Mayer, K. M.; Hafner, J. H. Localized Surface Plasmon Resonance Sensors. *Chem. Rev.* **2011**, *111*, 3828−3857.
(24) Zhang, Q.; Li, N.; Goebl, J.; Lu, Z.; Yin, Y. A Systematic Study of the Synthesis of Silver Nanoplates: Is Citrate a "Magic" Reagent? *J. Am. Chem. Soc.* **2011**, *133*, 18931−18939.
(25) Wang, J.; Luo, D.; Cai, Y.; Li, X.-L.; Chen, H.-Y.; Xu, J.-J. A plasmonic Au-Ag janus nanoprobe for monitoring endogenous hydrogen sulfide generation in living cells. *Biosens. Bioelectron.* **2022**, *213*, No. 114422.
(26) Tang, L.; Li, S.; Han, F.; Liu, L.; Xu, L.; Ma, W.; Kuang, H.; Li, A.; Wang, L.; Xu, C. SERS-active Au@Ag nanorod dimers for ultrasensitive dopamine detection. *Biosens. Bioelectron.* **2015**, *71*, 7−12.
(27) Vassalini, I.; Borgese, L.; Mariz, M.; Polizzi, S.; Aquilanti, G.; Ghigna, P.; Sartorel, A.; Amendola, V.; Alessandri, I. Enhanced Electrocatalytic Oxygen Evolution in Au-Fe Nanoalloys. *Angew. Chem.* **2017**, *129*, 6689.
(28) http://www.eshian.com/standards/33899.html (accessed September 1, 2022).
(29) Yu, J.; Qi, J.; Li, Z.; Tian, H.; Xu, X.-L. A Colorimetric Ag+ Probe for Food Real-Time Visual Monitoring. *Nanomaterials* **2022**, *12*, 1389.
(30) Xu, M.; Soliman, M. G.; Sun, X.; Pelaz, B.; Feliu, N.; Parak, W. J.; Liu, S. How Entanglement of Different Physicochemical Properties Complicates the Prediction of in Vitro and in Vivo Interactions of Gold Nanoparticles. *ACS Nano* **2018**, *12*, 10104−10113.
(31) Armao, J. J.; Nyrkova, I.; Fuks, G.; Osypenko, A.; Maaloum, M.; Moulin, E.; Arenal, R.; Gavat, O.; Semenov, A.; Giuseppone, N. Anisotropic Self-Assembly of Supramolecular Polymers and Plasmonic Nanoparticles at the Liquid−Liquid Interface. *J. Am. Chem. Soc.* **2017**, *139*, 2345−2350.
(32) Sawczyk, M.; Klajn, R. Out-of-Equilibrium Aggregates and Coatings during Seeded Growth of Metallic Nanoparticles. *J. Am. Chem. Soc.* **2017**, *139*, 17973−17978.
(33) James Singh, K.; Ahmed, T.; Gautam, P.; Sadhu, A. S.; Lien, D.-H.; Chen, S.-C.; Chueh, Y.-L.; Kuo, H.-C. Recent Advances in Two-Dimensional Quantum Dots and Their Applications. *Nanomaterials* **2021**, *11*, 1549.
(34) Ghareeb, R. Y.; Shams El-Din, N. G. E.-D.; Maghraby, D. M. E.; Ibrahim, D. S. S.; Abdel-Megeed, A.; Abdelsalam, N. R. Nematicidal activity of seaweed-synthesized silver nanoparticles and extracts against Meloidogyne incognita on tomato plants. *Sci. Rep.* **2022**, *12*, No. 3841.
(35) Devasia, D.; Wilson, A. J.; Heo, J.; Mohan, V.; Jain, P. K. A rich catalog of C−C bonded species formed in CO2 reduction on a plasmonic photocatalyst. *Nat. Commun.* **2021**, *12*, No. 2612.
(36) Lee, J.-S.; Kim, H.; Algar, W. R. Thiol-Ligand-Catalyzed Quenching and Etching in Mixtures of Colloidal Quantum Dots and Silver Nanoparticles. *J. Phys. Chem. C* **2017**, *121*, 28566−28575.
(37) Yu, K.; Li, M.; Chai, H.; Liu, Q.; Hai, X.; Tian, M.; Qu, L.; Xu, T.; Zhang, G.; Zhang, X. MOF-818 nanozyme-based colorimetric and electrochemical dual-mode smartphone sensing platform for in situ detection of H2O2 and H2S released from living cells. *Chem. Eng. J.* **2022**, *451*, 138321.
(38) Huang, X.; Sun, W.; Li, Z.; Shi, J.; Zhang, N.; Zhang, Y.; Zhai, X.; Hu, X.; Zou, X. Hydrogen sulfide gas sensing toward on-site monitoring of chilled meat spoilage based on ratio-type fluorescent probe. *Food Chem.* **2022**, *396*, No. 133654.
(39) Jiang, S.; Cui, C.; Bai, W.; Wang, W.; Ren, E.; Xiao, H.; Zhou, M.; Cheng, C.; Guo, R. Shape-controlled silver nanoplates colored fabric with tunable colors, photothermal antibacterial and colorimetric detection of hydrogen sulfide. *J. Colloid Interface Sci.* **2022**, *626*, 1051−1061.
(40) Zhang, F.; Shang, Y.; Yu, R.; Wang, Y.; Feng, F.; Guo, Q.; Xing, J.; Tian, Z.; Zeng, J.; Yan, Z. Cu2O induced Au nanochains for highly sensitive dual-mode detection of hydrogen sulfide. *J. Hazard. Mater.* **2022**, *436*, No. 129144.
(41) Rukchon, C.; Nopwinyuwong, A.; Trevanich, S.; Jinkarn, T.; Suppakul, P. Development of a food spoilage indicator for monitoring freshness of skinless chicken breast. *Talanta* **2014**, *130*, 547−554.

https://doi.org/10.1021/acsomega.2c05682
ACS Omega 2022, 7, 44215−44222